Journal of
Synchrotron Radiation

ISSN 0909-0495

Received 23 November 2004
Accepted 20 April 2005

In situ tensile testing of human aortas by time-resolved small-angle X-ray scattering

F. Schmid,[a,b] G. Sommer,[b] M. Rappolt,[a] C. A. J. Schulze-Bauer,[b]† P. Regitnig,[c] G. A. Holzapfel,[b] P. Laggner[a] and H. Amenitsch[a]*

[a]Austrian Academy of Science, Institute of Biophysics and X-ray Structure Research, Graz, Austria, [b]Graz University of Technology, Institute for Structural Analysis – Computational Biomechanics, Graz, Austria, and [c]Medical University Graz, Institute of Pathology, Graz, Austria.
E-mail: heinz.amenitsch@elettra.trieste.it

The collagen diffraction patterns of human aortas under uniaxial tensile test conditions have been investigated by synchrotron small-angle X-ray scattering. Using a recently designed tensile testing device the orientation and *d*-spacing of the collagen fibers in the adventitial layer have been measured *in situ* with the macroscopic force and sample stretching under physiological conditions. The results show a direct relation between the orientation and extension of the collagen fibers on the nanoscopic level and the macroscopic stress and strain. This is attributed first to a straightening, second to a reorientation of the collagen fibers, and third to an uptake of the increasing loads by the collagen fibers.

Keywords: human tissue; biomechanics; artery; small-angle X-ray scattering; collagen; fiber diffraction; tensile testing.

1. Introduction

According to the WHO World Health Report, cardiovascular diseases make up for roughly 30% of total global deaths (WHO, 2004). With a value of about 50%, the situation is even more alarming in developed countries (Petersen *et al.*, 2004; Statistik Austria, 2004). Major causes for cardiovascular disease are biochemical and biomechanical changes in the wall of a blood vessel or a narrowing of its diameter. This narrowing of the artery is the cause for 'classic' diseases such as ischemic stroke and heart attack. An increase in the diameter can be achieved by applying, for example, an angioplasty, which represents a mechanical solution for a clinical problem. It is the most frequent therapeutical intervention world wide (Fleisch & Meier, 1999) with great and steadily growing medical, socioeconomical and scientific interest (American Heart Association, 2003). Although this is meanwhile a standard procedure, there is still a lack of understanding of the detailed mechanisms during this treatment.

A profound description requires an in-depth knowledge of the function and interaction of the relevant biological tissues based on their (macro- and nano-) structure and mechanics. Elastomechanical and structural studies have been carried out mostly on tendons (Mosler *et al.*, 1985; Sasaki *et al.*, 1999; Fratzl *et al.*, 1998; Puxkandl *et al.*, 2002; Wess *et al.*, 1998; Orgel *et al.*, 2001; Parry & Craig, 1979; Parry, 1988; Castellani *et al.*, 1983; Marchini *et al.*, 1986). Few investigations have been performed on collagen-poor tissues such as rat skin or bovine perimysium (Purslow *et al.*, 1998). Measurements on blood vessels have been carried out on the basis of uniaxial and biaxial extensions tests or on inflation tests with internal pressure (Roveri *et al.*, 1980; Bigi *et al.*, 1981, 1984). However, animal tissue has been used.

Experiments on human arteries investigating the layer-specific macroscopic stress–strain behavior have been carried out by Holzapfel *et al.* (2004, 2005). These experiments on human tissue were sufficient to study the mechanical responses of the different arterial layers on the macroscopic level. However, they did not provide nanostructural information about the collagen orientation. In earlier studies, layer-specific tests on different animal arteries were carried out to relate smooth muscle fiber and collagen fiber orientation (Re *et al.*, 1979, 1980*a*,*b*). Collagen fiber orientations of different human arteries at constant stretch have been studied by the group of Canham using polarized light microscopy (Canham *et al.*, 1989, 1991, 1992; Finlay *et al.*, 1995, 1998; Rowe *et al.*, 2003). These studies provided approximate information about the orientation and the quantity of collagen fibers at the fixed states.

A thorough understanding of the macrostructural and nanostructural interaction under stress in arterial tissue is still missing. Eventually, macromolecular structural changes and their relation to physiology and pathology will be the key to clinical application. Many of the experiments mentioned above have been performed under non-physiological condi-

† Deceased December 2002.

tions and did not use human tissue. The tendon tests were mainly performed to understand the principal behavior of collagen itself. Some tests (Bigi *et al.*, 1981; Re *et al.*, 1979; Roveri *et al.*, 1980) provided 'snapshots' instead of continuous *in situ* information. Layer-specific quasi-static tests on human arterial tissue using time-resolved synchrotron radiation and related physical and numerical models provide information for the development of clinical applications.

In this *in situ* study, synchrotron radiation was used to investigate time-resolved changes in the orientation and *d*-spacing of collagen fibers in the individual layers of human aortas, which consist of three major layers. The results for two samples taken from the adventitia (the outermost layer) are presented here. The samples were cut from the same artery, one in the longitudinal and the other in the circumferential direction. The adventitia can be considered as a composite made up from extracellular matrix and embedded fibers, such as collagen and elastin fibers (see, for example, Silver *et al.*, 2001). The sketch in Fig. 1 shows the fiber alignment in the arteria according to Purslow *et al.* (1984). Our sample strips were measured in the radial direction only and were kept in a physiological environment during uniaxial tensile tests. Representative parameters such as force, displacement and lateral contraction were recorded simultaneously. Further details on the sample preparation, the descriptions of the tension cell and on the data analysis are given in §2. Results of the macrostructural and nanostructural changes during tensile testing are demonstrated with an example, and discussed in §3. Finally, a summary and an outlook is given in §4.

2. Materials and methods

2.1. Sample preparation

The arteries from human cadavers were excised during autopsy within 24 h from death and were frozen directly after they became available. Use of autopsy material from human subjects was approved by the Ethics Committee, Medical University Graz, Austria. Before preparation, the excised arteries were defrosted and stored in a 0.9% physiological saline solution at a temperature of 310 $\pm$ 0.1 K. The samples considered for testing were prepared on the day before the X-ray measurement.

The arteries were pruned from remaining connective tissues and cut in the axial direction to obtain a rectangular flat sheet. The layers were separated by pulling apart and, where necessary, through careful disconnection of the inter-connective tissue with a scalpel. The layer preparation process was not always successful since either macroscopic inspection or the prepared histological images inspected afterwards have proven that the result was not the desired single arterial layer. From these separated layer sheets, strips in axial and circumferential orientations were cut out with a sharp knife [for prepared strip samples see, for example, Fig. 3 of Holzapfel *et al.* (2004)].

Pieces of sandpaper were then attached to the ends of the strip samples for better clamping and to prevent slippage during testing. Two black markers were glued point-wise with cyanoacrylate adhesive gel (Henkel, Vienna, Austria) in parallel onto the middle part of the samples, which served as gauge markers for the axial deformation measurements with the video extensometer (Fig. 2). For representative tissue samples see, for example, Fig. 4 of Holzapfel *et al.* (2004). The thickness of the sample in the gauge region was measured before testing.

Also, during measurements the samples were immersed in a calcium-free 0.9% physiological saline solution at a temperature of 310 $\pm$ 0.1 K. Finally, after experimental testing and X-ray measurements, the samples were stored in alcohol for histological examinations.

2.2. Sample stage and mechanical measurements

The sample stage shown in Fig. 3 was designed specifically for uniaxial experiments. The sample was mounted inside the sample container (*c*) between two clamps (*d*). The upper clamp was mounted onto the 25 N load cell (*b*) (type F1/25N, class 1 according to DIN 51220, Messphysik, Fürstenfeld, Austria), which itself was attached to the M-126 motorized

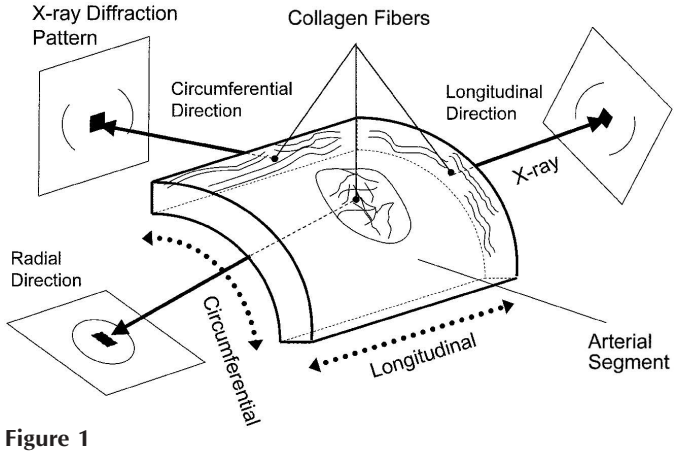

Figure 1
Sketch of an arterial segment and the embedded collagen fibers. The corresponding expected diffraction patterns of the meridional peak from the gap–overlap periodicity of collagen are shown for different directions. The collagen fibers are oriented in axial layers inside the arterial wall, but show no correlation between them in the radial direction. As a consequence, owing to the random orientation, an almost circular diffraction pattern is measured in the radial direction.

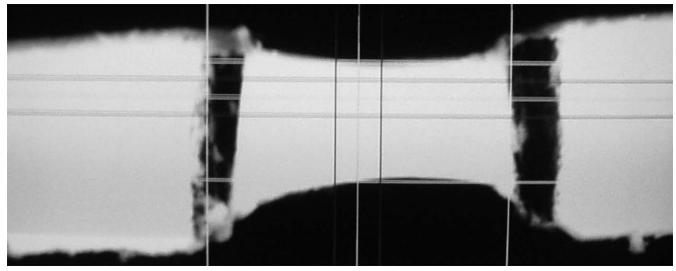

Figure 2
Stretching of a representative sample as viewed by the video-extensometer. The black vertical lines are the markers for length measurements ('length' is in the horizontal direction in the image).

linear translation stage (*a*) [Physikinstrumente (PI), Karlsruhe, Germany]. The minimum incremental motion was 0.1 μm and the maximum velocity was 1.5 mm s^{-1}. With the given travel range of 25 mm a maximum extension of at least 30% might be achieved. The sample container was made from a U-shaped stainless steel bar. The front plate was made from Plexiglas which, for sample mounting, could be easily attached and removed. Rubber sealings kept the tension cell leak proof. The back plate was made from stainless steel. Both plates contained circular-shaped X-ray windows (*f*), of which the distance was adjustable to minimize background scattering and absorption arising from water. These X-ray windows were made of 10 μm thin polyethylene-terephthalate film (Kalle GmBH, Wiesbaden, Germany), and were tested to give negligible contribution to the measured intensities. Two copper blocks (*e*) on either side of the container were used as a heat exchanger. The temperature was controlled by a water bath to within 0.1 K in the range 273–363 K (Unistat CC, Huber, Offenburg, Germany).

Prior to testing, the samples were subjected to cyclic loading and unloading until the typical stress softening effect diminished and the material exhibited an almost repeatable cyclic behavior (the material is then said to be 'pre-conditioned'). For the pre-conditioning of the present specimens it turned out that three loading–unloading cycles were sufficient. We have used a constant crosshead speed of <0.05 mm s^{-1}, and the final length was the same for all subsequent tests. After these three cycles the force at maximum elongation remains rather constant. The uniaxial extension tests documented in this work were performed as a displacement-driven process at a very slow constant speed (<0.05 mm s^{-1}).

An ME-46 video-extensometer (Messphysik, Fürstenfeld, Austria) determined online the change of length and width of an area in the middle of the sample. Using a 50 mm lens and an OS-65-D camera (Mintron, Taipei, Taiwan) with a frequency of 25 Hz a resolution of better than 1 μm was achieved.

The video-extensometer calculated the distance between the two black markers that were carefully attached onto the comparably bright sample set perpendicular to its length axis (Fig. 2). Two coldlight sources with optical fiber light guide illuminated the sample and the surrounding area to give a bright and contrast-rich image for the video-extensometer camera. The edge of the bright sample and the dark background defined another pair of lines that were analyzed by the video-extensometer to measure the lateral contraction.

Fig. 4 shows the set-up of the measurement schematically. A visible image of the sample was reflected by a mirror to the video-extensometer camera. Correction for the distortion of the video-extensometer image, caused by the position of the mirror, was performed. For further details concerning the X-ray set-up, see §2.3.

All instruments and process variables of the sample stage were controlled and logged, respectively, by a PC using specifically developed programs in *LabView* (National Instruments, Austin, TX, USA).

2.3. X-ray measurements

All diffraction patterns were recorded at the Austrian SAXS beamline at ELETTRA, Trieste (Amenitsch *et al.*, 1998; Bernstorff *et al.*, 1998) using a two-dimensional image-intensified CCD detector (Model CV 12, Photonic Science, Millham, UK). The sample-to-detector distance was set to 2.3 m to cover the corresponding *s*-range [$s = 2\sin(\Theta)/\lambda$, where Θ is the Bragg angle and λ is the X-ray wavelength] of interest from about 1/980 $Å^{-1}$ to 1/55 $Å^{-1}$ at an X-ray energy of 8 keV. The angular calibration of the detector was performed with dry rat-tail tendon, which has a *d*-spacing of 640 Å (Bigi & Roveri, 1991). Two images taken with rat-tail collagen oriented in the horizontal and vertical direction were used to determine the beam center.

During the time course of the mechanical stretch and release the diffraction patterns were recorded continuously with an integration time of about 10 s each depending on the scattering power of the samples.

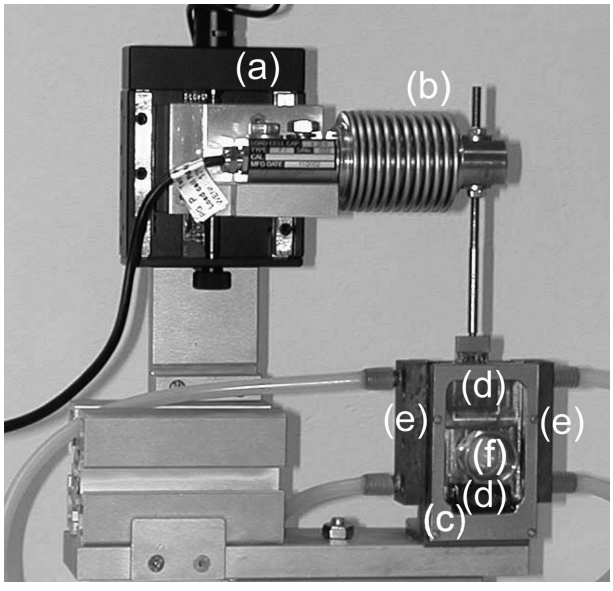

Figure 3
Tension cell: the sample is mounted between two clamps (*d*), of which the upper is moved by a translation stage (*a*). Force is measured using a load cell (*b*), on which the upper clamp is mounted.

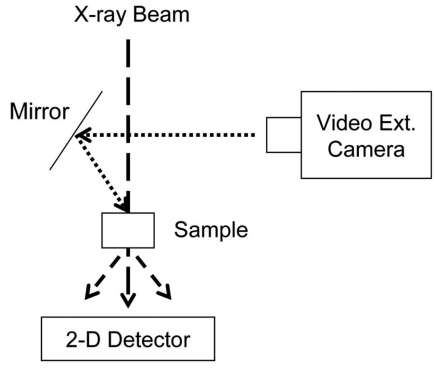

Figure 4
Schematic drawing of the set-up as installed in the beamline.

2.4. Data analysis

All the SAXS images were corrected for electronic dark noise, spatial distortion and detector efficiency. Furthermore, they were transformed from Cartesian (Q_X, Q_Z) into polar coordinates with radial component Q_R and azimuthal angle φ, see also Fig. 5 (Purslow *et al.*, 1998), as prior suggested by Roveri *et al.* (1980). This data reduction was performed using the software package *Fit2D* (Hammersley *et al.*, 1995). All the following steps were performed using specially developed routines written in *Mathematica* (Wolfram Research, Champaign, USA). The images were normalized for intensity fluctuations of the primary beam, and occasional 'zingers' were eliminated using a median filter.

After the background was subtracted by fitting third-order polynomials to the intense third-order Bragg peak, the resulting peak data were analyzed both in the azimuthal and radial directions. Therefore a boxed area around the peak was integrated in the desired directions (compare inset of Fig. 5). The first outcome represents the azimuthal intensity distribution, whereas the center of the radial intensity distribution was used for the determination of the *d*-spacing. For intensity distributions of one complete experiment, all the corresponding frames were assembled and smoothed with a median and a 'Lee' filter (Lee, 1986). Both the azimuthal and the radial distributions were fitted with Gaussians.

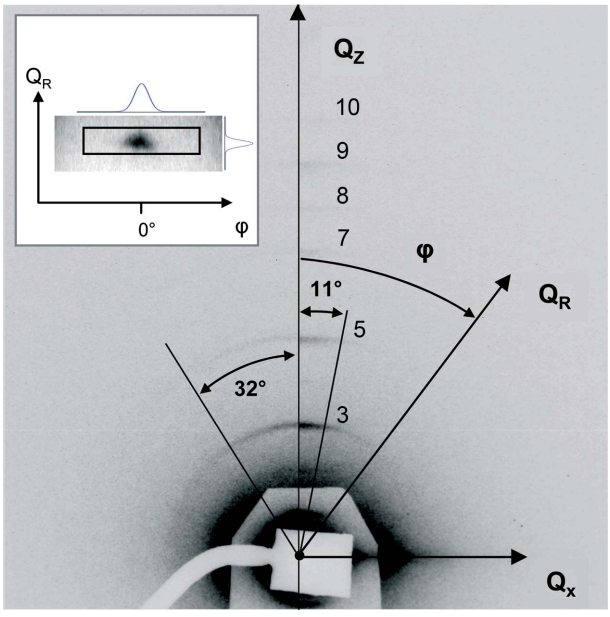

Figure 5
Typical diffraction patterns of an unstretched, not pre-conditioned (left) and a stretched (right) adventitia cut in the circumferential direction. The load axis is in the Q_Z direction. The strongest meridional peaks of collagen are indicated by their orders. The half width at half-maximum (HWHM) of the azimuthal intensity distributions are given explicitly for both load cases in the corresponding diffraction pattern. Furthermore, the transformation from Cartesian (Q_X, Q_Z) into polar (Q_R, φ) coordinates is indicated. In the inset the third-order reflection of the stretched adventitia is represented in polar coordinates. The boxed region indicates the area for the radial and azimuthal integration, respectively. The peak shapes in both the φ and Q_R directions are almost Gaussian.

The force F and the geometrical parameters of the sample delivered from the video-extensometer, *i.e.* the current sample length L and the current sample thickness W, are used to calculate stress and strain of the different specimens. Knowing the initial sample volume $V_0 = L_0 W_0 T_0$, in uniaxial extension tests the current stress σ is given by

$$\sigma = FL/L_0 W_0 T_0, \tag{1}$$

where L_0, W_0 and T_0 denote the initial length, width and thickness of the sample, respectively. The strain ε is defined as

$$\varepsilon = (L - L_0)/L_0. \tag{2}$$

During elongation the thickness T of the sample decreases, and hence also the diffracted intensity diminishes. This effect has been accounted for by normalizing the intensity I to the sample thickness,

$$\tilde{I} = I/T \propto ILW, \tag{3}$$

where $\tilde{I}$ is the normalized intensity.

3. Results and discussion

Measurements were carried out on all samples (in the longitudinal and circumferential directions) obtained from the three layers of the excised aortas. The results presented here refer to two samples taken from the adventitia along the longitudinal and the circumferential directions.

Two representative static X-ray diffraction patterns for the adventitial sample in the circumferential direction are shown in Fig. 5, which were recorded before pre-conditioning (left) and at maximum stretch in the last pre-condition cycle (right). The diffraction patterns display an intensity distribution which is typical for wet connective tissue samples containing collagen fibers (type I and III). The *d*-spacing of the collagen structure was quantified to be 654 Å in the unloaded state after pre-conditioning which agrees well with the value determined by Folkhard *et al.* (1987). Generally, in the unstretched state, the collagen fibers in the sample are rather homogeneously distributed as seen in the broad arch of the third-order reflection (left), whereas at the maximum stretch (right) an orientation of the fibers towards the load axis is apparent (small arch). To quantify the orientation of the fibers the azimuthal intensity distribution of the strong third-order peak has been analyzed as shown in the inset of Fig. 5 (see also §2.4). In the unstretched state (left-hand side in Fig. 5) the full width at half-maximum (FWHM) of the azimuthal intensity distribution $\Delta\varphi$ has a value of 63.9°, which decreases to 21.9° for the stretched sample (right-hand side in Fig. 5).[1] After pre-conditioning, the FWHM of the relaxed sample is 56.2°. For the longitudinal sample, the corresponding values were determined to be 86.8°, 38.1° and 78.9°, respectively. Thus, pre-conditioning, the requirement to reach steady-state mechanical conditions, results already in a pronounced alignment of the collagen fibers towards the applied force.

[1] Note that, for sake of clarity, HWHM values are given in Fig. 5.

During a dynamic measurement the general behavior of the mechanical parameters are demonstrated in Fig. 6(*a*). With elongation of the sample, the force increases and the sample undergoes lateral contraction (width and thickness). On release, the inverse phenomena are observed.

For a series of diffraction patterns (about 200 frames) recorded during the tensile test (load/unload) the azimuthal intensity distribution of the third-order reflection is extracted to obtain the fiber orientation *in situ*. The result is presented in Fig. 6(*b*) for a strip oriented in the longitudinal direction. During elongation of the sample a continuous alignment of the collagen fibers in the loading direction can be observed, *i.e.* the azimuthal intensity distribution clearly narrows.

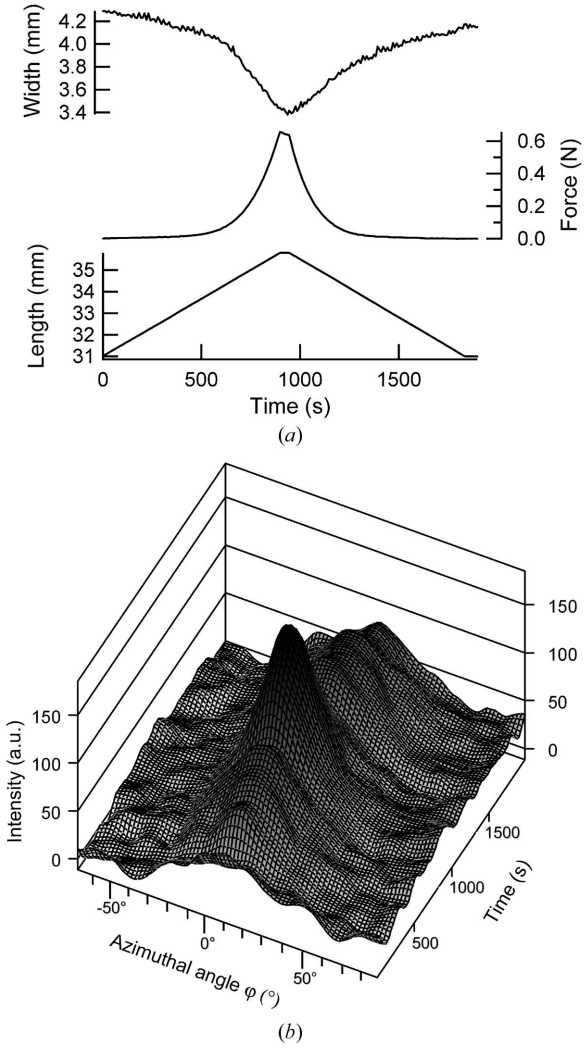

Figure 6
(*a*) Typical time course of width, force and length during a tensile test. A circumferential adventitia was stretched at constant speed corresponding to an initial strain rate of 0.005 min^{-1}. At maximum extension a strain of about 0.2 was reached. (*b*) Azimuthal intensity distribution of the third-order Bragg peak during a complete cycle. After about 1000 s the maximum load is reached, and the azimuthal intensity distribution is clearly sharper than at the beginning of the experiment (no load), *i.e.* the fiber orientation has reached its maximum at this point (compare also with Fig. 5). Thereafter the fibers become relaxed (time >1000 s) and the azimuthal intensity distribution smears out again.

The two stress–strain plots of a loading/unloading cycle of adventitia samples in circumferential and longitudinal directions are shown in Fig. 7. Similar to tendon and other soft biological tissues, there is a toe region at low strains, in which strain increases without a significant increase in stress. This is followed by a heel region, when stress increases, and finally turns into a locking region at high strains, which is due to the stiffening of the collagen fibers in the tissue (see, for example, Misof *et al.*, 1997; Holzapfel, 2001). The slight hysteresis is typically seen in tensile tests of soft biological materials and is caused by small viscoelastic effects remaining after preconditioning.

To assess the qualitative observation of Fig. 6(*b*), the FWHM of the azimuthal intensity distribution $\Delta\varphi$, *i.e.* the degree of the collagen fiber orientation in the load direction, is given for both strips in Fig. 8.

From the azimuthal integration of the third-order peaks the change of the collagen *d*-spacing has been determined. The

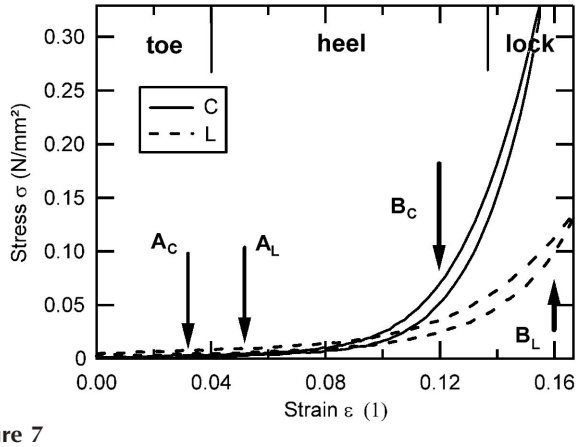

Figure 7
Stress–strain plots (loading and unloading) for two samples of an adventitia tested in the circumferential (C) and in the longitudinal (L) directions. Three ranges of the stress–strain plots are indicated: toe (up to *A*), heel (ranging between *A* and *B*) and lock (larger than *B*). A_C, B_C and A_L, B_L give the ranges for the circumferential and the longitudinal directions, respectively.

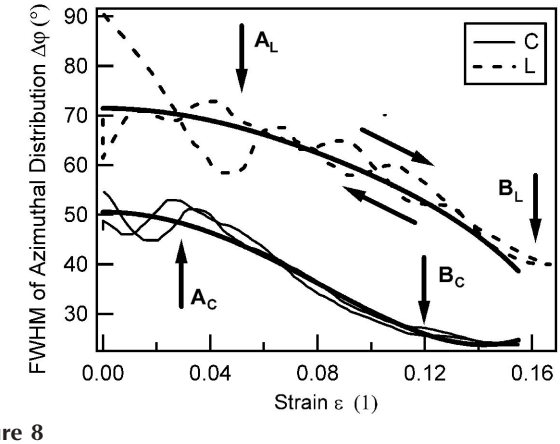

Figure 8
FWHM of the azimuthal intensity distribution $\Delta\varphi$ of a circumferential (C) and a longitudinal (L) adventitial sample as a function of strain ε for a loading/unloading cycle. The points *A* and *B* identifying the three regions of the stress–strain plot are indicated as in Fig. 7.

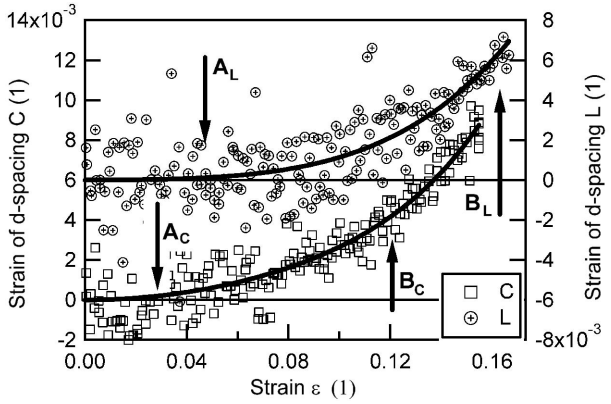

Figure 9
Strain of collagen *d*-spacing as a function of the strain ε for a circumferential (C) and longitudinal (L) adventitial sample. The nomenclature for the points *A* and *B* is the same as in Figs. 7 and 8.

correlation between the increase of the fibrillar strain, *i.e.* the relative increase of the collagen *d*-spacing, and the macroscopic strain ε is shown in Fig. 9 again for a complete cycle. The result is qualitatively similar to the macroscopic measured stress–strain curve (Fig. 7). Comparing Figs. 7, 8 and 9, the regions (toe, heel, lock) can be identified and are discussed in the following.

In the toe region (until A_C, A_L) all curves show just weak dependencies on the strains. The extension is mainly caused by a macroscopic extension of the elastin in the matrix material. Moreover, a microscopic straightening of the wavy collagen fibers appears (wave period about 100 µm). This is discussed for tendon collagen in the toe region by Fratzl *et al.* (1998) and for biological tissue by Holzapfel (2001).

At the macroscopic strains ε indicated by A_C and A_L (heel region), the collagen fibers start to reorient themselves into the load direction driven by the extension of the matrix material, as it is evidenced by the continuous decrease of the fiber distribution's FWHM $\Delta\varphi$ (Fig. 8). This relation of the FWHM *versus* the strain ε was also found by Roveri *et al.* (1980). Around this point the fibers start to contribute to the stress, as can be observed in the increase of the fiber strain (Fig. 9), although the macroscopic stress σ still remains relatively small compared with the stress reached in the locking domain (Fig. 7).

At the points indicated by B_C and B_L in Figs. 7 and 8 (locking domain), the collagen fibers reach their maximum orientation. The load is transferred from the elastin fibers to the collagen fibers, which leads to the stiffening of the adventitia.

In general, as seen from Fig. 9, the fibrillar strain is about one order of magnitude smaller than the macroscopic strain ε over the loading/unloading domain for both samples. This supports the assumption reported in the literature (*e.g.* Purslow *et al.*, 1998) that the macroscopic strain is only partly determined by the fiber strain. Consequently the elongation of the matrix material, in which the collagen fibers are embedded, is the main cause for the macroscopic strain. This is also found in studies by Fratzl *et al.* (1998) and Sasaki & Odajima (1996) for tendon collagen, in which the proteoglycan matrix is mainly responsible for the extension. In particular, for soft biological tissue, the nanostrain/macrostrain relation has been discussed by Purslow *et al.* (1998) and Bigi *et al.* (1981). The authors conclude that the matrix material, as in our case, is the main factor for the macroscopic strain.

Comparing the data obtained from the circumferential and longitudinal samples, an important finding is that the degree of collagen fiber orientation (Fig. 8) is directly related to the stiffness of the arterial tissue (Fig. 7). The increased stiffness in the locking region of the circumferential adventitia is caused by the increased alignment of the collagen fibers into the load direction [25° circumferential against 40° for the longitudinal direction in the stretched condition (Fig. 8)]. This predominant alignment of the collagen fibers, and consequently the increased stiffness, in the circumferential direction was also attributed to the fact (Bigi *et al.*, 1981) that for a cylinder geometry under inflation pressure load the circumferential stress is twice the longitudinal stress (law of Laplace). Therefore, for the adventitia, the *in vivo* stresses occurring in a blood vessel match the material requirements for stiffness in the corresponding directions.

4. Conclusion and outlook

Biomechanics of arteries cover almost nine orders of magnitude in size: vessels have to withstand mechanical deformation in the millimeter regime, straightening of embedded fibers occurs on a microscopical level, and the collagen fiber stretches on a nanoscopic scale. The presented method and the data of this study demonstrate the unique possibility of synchrotron radiation to investigate this complex nanoscopic and macroscopic interplay during tensile testing experiments of biological soft tissues *in situ*. The three distinct regions of the macroscopic measured stress–strain diagram (heel, toe, lock) are explained by fiber straightening, fiber reorientation and fiber strain on the nanoscopic scale. This multilevel analysis is an essential pre-requisite to understanding the overall mechanisms in loaded biological tissues.

At present a thorough analysis of the quasi-static data of all samples from the three layers is under way, and will be documented elsewhere. Nevertheless, a next step is to focus on the investigation of the viscoelastic phenomena of human soft tissues, as they occur during relaxation and creep tests. Another important perspective will be the study of the rupture behavior of human soft tissues in order to investigate the related damage/failure mechanism on the nanoscopic scale. As the ultimate goal we aim to contribute to the mathematical formulation of the existing constitutive arterial models, which may enable numerical simulations of arteries on layer-specific and nanostructural biophysical models.

Financial support for this research was provided by the ''Fonds zur Fortsetzung von Christian's Forschung'', the Austrian Science Foundation under START-Award Y74-TEC, and by ELETTRA/European Community under Research

Infrastructure Action FP6 (contract: RII3-CT-2004-506008 IA-SFS). These supports are gratefully acknowledged.

References

Amenitsch, H., Rappolt, M., Kriechbaum, M., Mio, H., Laggner, P. & Bernstorff, S. (1998). *J. Synchrotron Rad.* **5**, 506–508.

American Heart Association (2003). *Heart Disease and Stroke Statistics – 2004 Update.* American Heart Association, Dallas, TX, USA.

Bernstorff, S., Amenitsch, H. & Laggner, P. (1998). *J. Synchrotron Rad.* **5**, 1215–1221.

Bigi, A., Ripamonti, A. & Roveri, N. (1981). *Int. J. Biol. Macromol.* **3**, 287–291.

Bigi, A., Ripamonti, A. & Roveri, N. (1984). *Int. J. Biol. Macromol.* **6**, 21–25.

Bigi, A. & Roveri, N. (1991). *Handbook on Synchrotron Radiation*, Vol. 4, edited by S. Ebashi, M. Koch and E. Rubenstein. Amsterdam: Elsevier Science.

Canham, P. B., Finlay, H. M., Dixon, J. G., Boughner, D. R. & Chen, A. (1989). *Cardiovasc. Res.* **23**, 973–982.

Canham, P. B., Talman, E. A., Finlay, H. M. & Dixon, J. G. (1991). *Connect. Tissue Res.* **26**, 121–134.

Canham, P. B., Whittaker, P., Barwick, S. E. & Schwab, M. E. (1992). *Can. J. Physiol. Pharmacol.* **70**, 296–305.

Castellani, P. P., Morocutti, M., Franchi, M., Ruggeri, A., Bigi, A. & Roveri, N. (1983). *Cell Tissue Res.* **234**, 735–743.

Finlay, H. M., McCullough, L. & Canham, P. B. (1995). *J. Vasc. Res.* **32**, 301–312.

Finlay, H. M., Whittaker, P. & Canham, P. B. (1998). *Stroke*, **29**, 1595–1601.

Fleisch, M. & Meier, B. (1999). *Cardio. Rev.* **7**, 215–218.

Folkhard, W., Christmann, D., Geercken, W., Knorzer, E., Koch, M. H., Mosler, E., Nemetschek-Gansler, H. & Nemetschek, T. (1987). *Z. Naturforsch. C*, **42**, 1303–1306.

Fratzl, P., Misof, K., Zizak, I., Rapp, G., Amenitsch, H. & Bernstorff, S. (1998). *J. Struct. Biol.* **122**, 119–122.

Hammersley, A. P., Svensson, S. O., Thompson, A., Graafsma, H., Kvick, Å. & Moy, J. P. (1995). *Rev. Sci. Instrum.* **66**, 2729–2733.

Holzapfel, G. A. (2001). *Biomechanics of Soft Tissue*, in *The Handbook of Materials Behavior Models*, Vol. III, *Multiphysics Behaviors*, ch. 10, *Composite Media, Biomaterials*, edited by J. Lemaitre, pp. 1049–1063. Boston: Academic Press.

Holzapfel, G. A., Sommer, G., Gasser, T. C. & Regitnig, P. (2005). *Am. J. Physiol. Heart Circ. Physiol.* In the press.

Holzapfel, G. A., Sommer, G. & Regitnig, P. (2004). *J. Biomech. Eng.* **126**, 657–665.

Lee, J. S. (1986). *Opt. Eng.* **25**, 636–646.

Marchini, M., Morocutti, M., Ruggeri, A., Koch, M. H., Bigi, A. & Roveri, N. (1986). *Connect. Tissue Res.* **15**, 269–281.

Misof, K., Rapp, G. & Fratzl, P. (1997). *Biophys. J.* **72**, 1376–1381.

Mosler, E., Folkhard, W., Knorzer, E., Nemetschek-Gansler, H., Nemetschek, T. & Koch, M. H. (1985). *J. Mol. Biol.* **182**, 589–596.

Orgel, J. P., Miller, A., Irving, T. C., Fischetti, R. F., Hammersley, A. P. & Wess, T. J. (2001). *Structure*, **9**, 1061–1069.

Parry, D. A. (1988). *Biophys. Chem.* **29**, 195–209.

Parry, D. A. & Craig, A. S. (1979). *Nature (London)*, **282**, 213–215.

Petersen, S., Peto, V. & Rayner, M. (2004). *Coronary Heart Disease Statistics*, 2004 edition. British Heart Foundation, London, UK.

Purslow, P. P., Bigi, A., Ripamonti, A. & Roveri, N. (1984). *Int. J. Biol. Macromol.* **6**, 21–25.

Purslow, P. P., Wess, T. J. & Hukins, D. W. (1998). *J. Exp. Biol.* **201**, 135–142.

Puxkandl, R., Zizak, I., Paris, O., Keckes, J., Tesch, W., Bernstorff, S., Purslow, P. & Fratzl, P. (2002). *Philos. Trans. R. Soc. Lond. B*, **357**, 191–197.

Re, G., Bigi, A., Dalla, S. A., Incerti, A. & Roveri, N. (1979). *Boll. Soc. Ital. Biol. Sper.* **55**, 2149–2152.

Re, G., Bigi, A., Incerti, A. & Roveri, N. (1980*a*). *Boll. Soc. Ital. Biol. Sper.* **56**, 263–267.

Re, G., Bigi, A., Incerti, A. & Roveri, N. (1980*b*). *Boll. Soc. Ital. Biol. Sper.* **56**, 268–272.

Roveri, N., Ripamonti, A., Pulga, C., Jeronimidis, G., Purslow, P. P., Volpin, D. & Gotte, L. (1980). *Makromol. Chem.* **181**, 1999–2007.

Rowe, A. J., Finlay, H. M. & Canham, P. B. (2003). *J. Vasc. Res.* **40**, 406–415.

Sasaki, N. & Odajima, S. (1996). *J. Biomech.* **29**, 1131–1136.

Sasaki, N., Shukunami, N., Matsushima, N. & Izumi, Y. (1999). *J. Biomech.* **32**, 285–292.

Silver, F. H., Horvath, I. & Foran, D. J. (2001). *Crit. Rev. Biomed. Eng.* **29**, 279–301.

Statistik Austria (2004). *Jahrb der Gesundheitsstatistik 2002.* Statistik Austria.

Wess, T. J., Hammersley, A. P., Wess, L. & Miller, A. (1998). *J. Struct. Biol.* **122**, 92–100.

WHO (2004). *The World Health Report*, http://www.who.int/dietphysicalactivity/publications/facts/cvd/en/.